Supporting Information: Enhanced intersystem crossing and transient electron spin polarization in a photoexcited pentacene-trityl radical

Claudia E. Avalos,[a] Sabine Richert,[b,c] Etienne Socie,[a] Ganesan Karthikeyan,[d] Gilles Casano,[d] Gabriele Stevanato,[a] Dominik J. Kubicki,[a] Jacques E. Moser,[a] Christiane R. Timmel,[b] Moreno Lelli,[e,f] Aaron J. Rossini,[a,g] Olivier Ouari,[d] and Lyndon Emsley[a]

[a] Institut des Sciences et Ingénierie Chimiques, Ecole Polytechnique Fédérale de Lausanne (EPFL), CH-1015 Lausanne, Switzerland. Email : lyndon.emsley@epfl.ch

[b] Centre for Advanced Electron Spin Resonance (CAESR), University of Oxford, South Parks Road, Oxford OX1 3QR, U.K.

[c] Present address: Institute of Physical Chemistry, University of Freiburg, Albertstraße 21, 79104 Freiburg, Germany.

[d] Aix Marseille Univ, CNRS, ICR, Marseille, France.

[e] Center of Magnetic Resonance (CERM), University of Florence Via Luigi Sacconi 6, 50019 Sesto Fiorentino, Italy.

[f] Department of Chemistry "Ugo Schiff", University of Florence, Via della Lastruccia 3, 50019 Sesto Fiorentino, Italy.

[g] Present address: Iowa State University, Department of Chemistry, Ames, Iowa 50011, United States.

Table of Contents

1. Synthesis and Characterization of Pentacene Derivatives

All compounds investigated in this study were synthesized according to the procedures outlined below, with the exception of 6,13-bis((triethylsilyl)ethynyl)pentacene (pTES) **10**, which were purchased from Sigma-Aldrich.

1.1 Syntheses

General procedures: Unless otherwise noted, all reactions were carried out under an inert atmosphere of argon. Chemicals were used as received from the suppliers (Aldrich, TCI & Alfa Asear). Reactions were monitored by thin-layer chromatography (TLC) analysis. Column chromatography was carried out on silica gel (230-400 mesh). The 1H NMR spectra were recorded on a Bruker AVL spectrometer at 300 MHz and 13C NMR spectra were recorded at 75 MHz. The chemical shifts are reported in ppm downfield relative to TMS and referenced using the residual $CHCl_3$ resonance (δ = 7.26) for ^{1}H NMR and the central $CDCl_3$ resonance (δ = 77.16) for ^{13}C NMR. ESI-HRMS were performed on a SYNAPT G2 HDMS (Waters). The NMR and MS analysis were performed at the Spectropole facilities, Marseille. Pentacen-6-one derivative **1**[1] BDPA derivative **6**[2] and Trityl derivative **3**[3] were prepared as reported previously.

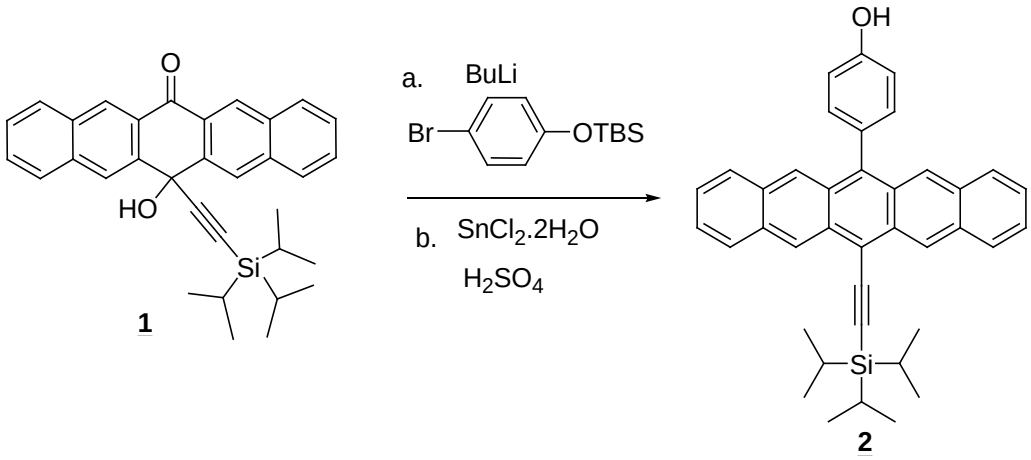

To a solution of (4-Bromophenoxy)-*tert*-butyldimethylsilane (2.15g, 7.5 mmol) in THF (20 mL) cooled to –78 °C was added dropwise BuLi (2.5 M in hexanes, 3.0 mL, 7.5 mmol). The solution was allowed to stir for 30 min. The mixture was transferred slowly via cannula into a solution of **1** (1.47 g, 3.0 mmol) in dry THF (20 mL) at –78 °C. The reaction mixture was allowed to warm to RT and stirred for 16 h, then cooled to 0 °C and quenched with satd. aq. NH_4Cl (100 mL) and extracted with CH_2Cl_2 (2 x 100 mL). The organic phase was washed with satd. aq. NaCl (100 mL), dried with Na_2SO_4 and the solvent removed in vacuo to get crude diol.

The crude intermediate was dissolved in THF (50 mL), and $SnCl_2$, $2H_2O$ (2.03 g, 9.0 mmol) and 10% aq. sulfuric acid (5.00 mL) were added and stirred at RT for 18hrs in the absence of light by covered the flask with aluminum foil. The reaction mixture was quenched with satd. aq. NH_4Cl and extracted with CH_2Cl_2 (3 x 60 mL). The combined organic phases was washed with H_2O (200 mL) and brine (200 mL), dried over Na_2SO_4, concentrated in vacuum and purified by flash chromatography to give **2** as a deep blue solid (0.25 g, 15% for 2 steps) and OTBS protected derivative **9** (0.5 g, 25% for 2 steps) which was converted to **2** in acidic condition (20% H_2SO_4 /THF) OTBS deprotection. R_f = 0.32 (Pentane/EtOAc: 7:3); ^{1}H NMR for **2** (CD_3Cl_3, 400 MHz, 25 °C) δ = 9.40 (s, 2H), 8.83 (s, 1H), 8.48 (s, 2H), 8.01 (d, *J* = 8.44 Hz, 2H), 7.90 (d, *J* = 8.56 Hz, 2H), 7.47 (d, *J* = 6.6 Hz, 4H), 7.38 (t, *J* = 7.0 Hz, 2H), 7.25 (d, *J* = 7.0 Hz, 2H), 1.50-1.44 (m, 21H) ppm; ^{13}C ($CDCl_3$, 75 MHz, 25 °C) δ = 155.3, 138.1,

132.8, 131.9, 131.4, 131.0, 128.8, 128.6, 128.5, 126.3, 125.8, 125.7, 125.3, 117.0, 115.5, 105.1, 104.9, 19.0 11.7 ppm; HRMS-ESI of comp **2**: m/z $[M+H]^+$calculated for $C_{39}H_{39}OSi^+$: 551.2765; found: 551.2764. HRMS-ESI of comp **9**: m/z $[M+H]^+$calculated for $C_{45}H_{53}OSi_2^+$: 665.3630; found: 665.3627.

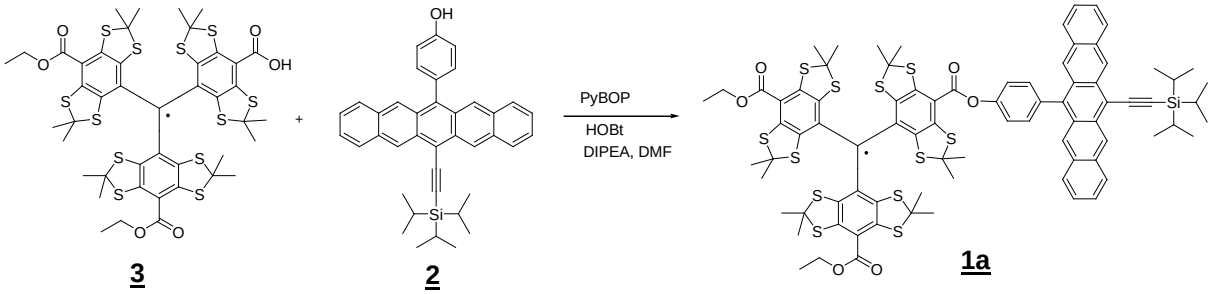

3 **2** **1a**

To a solution of trityl radical **3** (15 mg, 0.014 mmol) and pentacene derivative **2** (9.2 mg, 0.0168 mmol) in dry DMF (2 mL) was added PyBOP (19 mg, 0.035 mmol) and HOBt (4 mg, 0.035 mmol) followed by DIPEA (6 µL, 0.035 mmol).The reaction mixture was stirred at RT for 16 hrs and DMF was removed by vacuo and purified by SiO_2 column chromatography to obtain compound **pTrityl 1a** in 49% yield (11 mg); R_f = 0.5 (DCM); HRMS-ESI: m/z $[M+H]^+$calculated for $C_{83}H_{84}O_6S_{12}Si^{\cdot+}$: 1588.2680; found: 1588.2270.

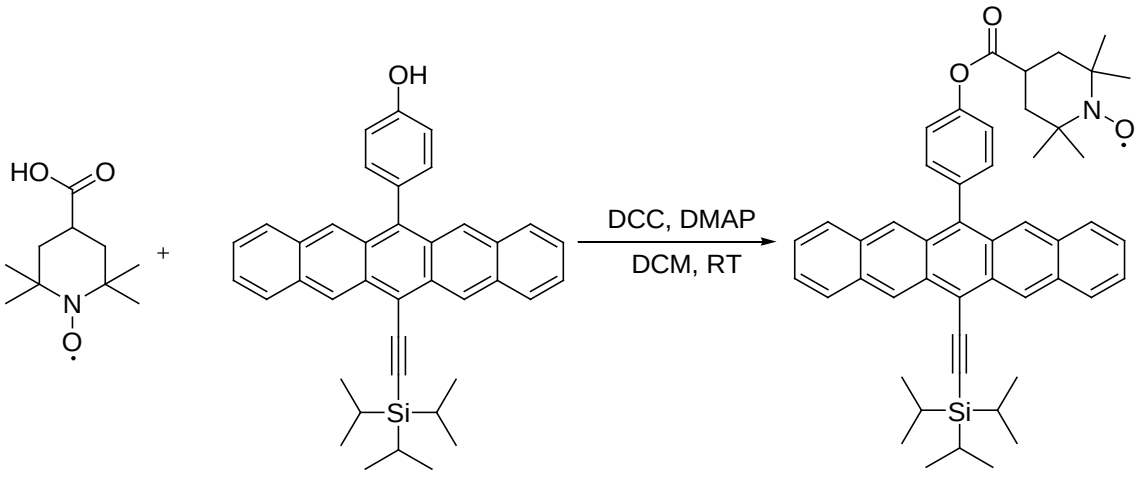

2 **2a**

To a solution of 4-Carboxy TEMPO (15 mg, 0.073 mmol) in DCM (2 mL) were added DCC (15 mg, 0.076 mmol), Pentacene derivative **2** (21 mg, 0.038 mmol) and DMAP (4 mg, 0.038 mmol). After stirring at RT for 16 hrs the reaction mixture was concentrated under reduced pressure and purified by flash chromatography to give ester **pTEMPO 2a** (11 mg, 40%), R_f = 0.41 (Pentane/EtOAc: 7:3); HRMS-ESI: m/z $[M+H]^+$ calculated for $C_{49}H_{55}NO_3Si^{+\cdot}$ 733.3946; found: 733.3946.

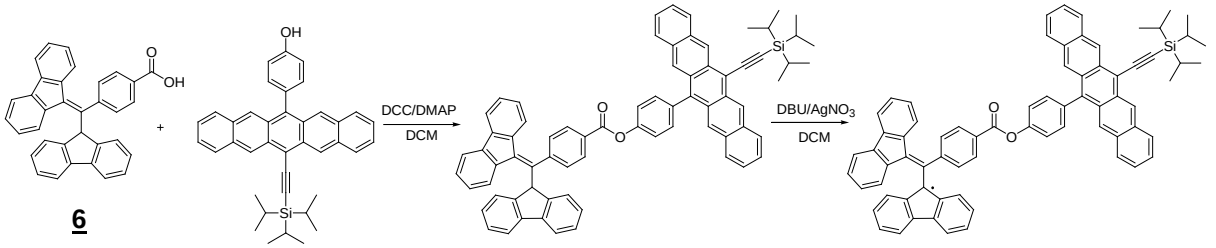

6 **2** **7** **3a**

To a solution of acid **6** (46 mg, 0.1 mmol, 1 equiv.) in DCM (2 mL) were added DCC (20 mg, 0.1 mmol, 1.0 equiv.), Pentacene derivative **2** (55 mg, 0.32 mmol, 1 equiv.) and DMAP (6 mg, 50 mol %). After stirring at RT for 16 hrs the reaction mixture was concentrated under reduced pressure and purified by flash chromatography to give ester **7** (60 mg, 60%), R_f = 0.8 (Pentane/EtOAc: 8:2);

^{1}H NMR of **7** ($CDCl_3$, 300 MHz, 25 °C) δ = 9.37 (s, 2H), 8.47 (d, J = 8.25 Hz, 1H), 8.29 (s, 2H), 7.97-7.89 (m, 4H), 7.79-7.76 (m, 3H), 7.72-7.63 (m, 4H), 7.60-7.48 (m, 5H), 7.42-7.27 (m, 12H), 6.92-6.81 (m, 2H), 6.59 (s, 1H), 6.03 (d, J = 8.16 Hz, 1H), 1.40-1.28 (m, 21H)ppm; ^{13}C ($CDCl_3$, 75 MHz, 25 °C) δ = 164.9, 150.7, 144.4, 143.7, 143.3, 142.0, 141.4, 140.0, 138.8, 138.5, 136.5, 136.3, 132.6, 131.9, 131.5, 129.7, 129.0, 128.9, 128.6, 128.5, 127.8, 127.7, 127.4, 127.1, 126.7, 125.9(x2), 125.3, 125.4, 125.3, 125.2, 123.4, 121.8, 120.2, 120.1, 120.0, 119.3, 115.9, 109.7, 108.5, 107.1, 103.1, 52.4, 19.0, 11.7 ppm; HRMS-ESI: m/z $[M+H]^+$calculated for $C_{73}H_{59}O_2Si^+$: 995.4279; found: 995.4280.

The ester **7** (32 mg, 0.03 mmol) and DBU (0.022 mL, 0.15 mmol) was taken in 2 mL DCM and stirred at RT for 30 min. $AgNO_3$ (0.06 mL, 0.06 mmol, 1 M solution in CH_3CN) was added and stirred at RT for 30 min. The reaction mixture was filtered and concentrated under reduced pressure. The crude product was purified by flash chromatography to yield **pBDPA 3a** (20 mg / 67 %), R_f = 0.37 (Pentane/EtOAc: 9:1); HRMS-ESI: m/z $[M+H]^+$ calculated for $C_{73}H_{58}O_2Si^{+\cdot}$ 994.4201; found: 994.4204.

1.2 Characterization: NMR, ESI-HRMS, CW EPR

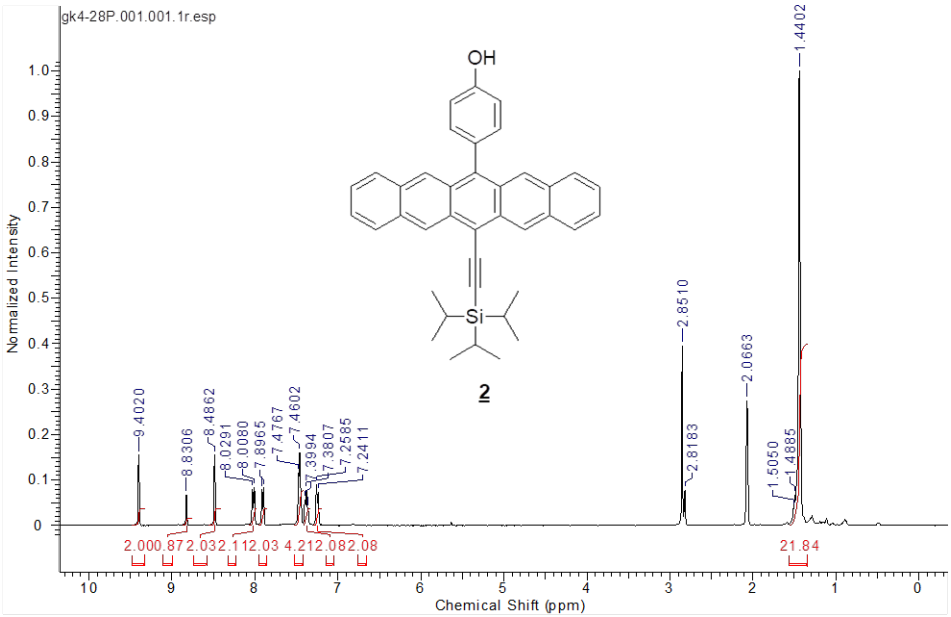

Figure S1: ^{1}H NMR (300 MHz, $CDCl_3$) spectrum of **2**.

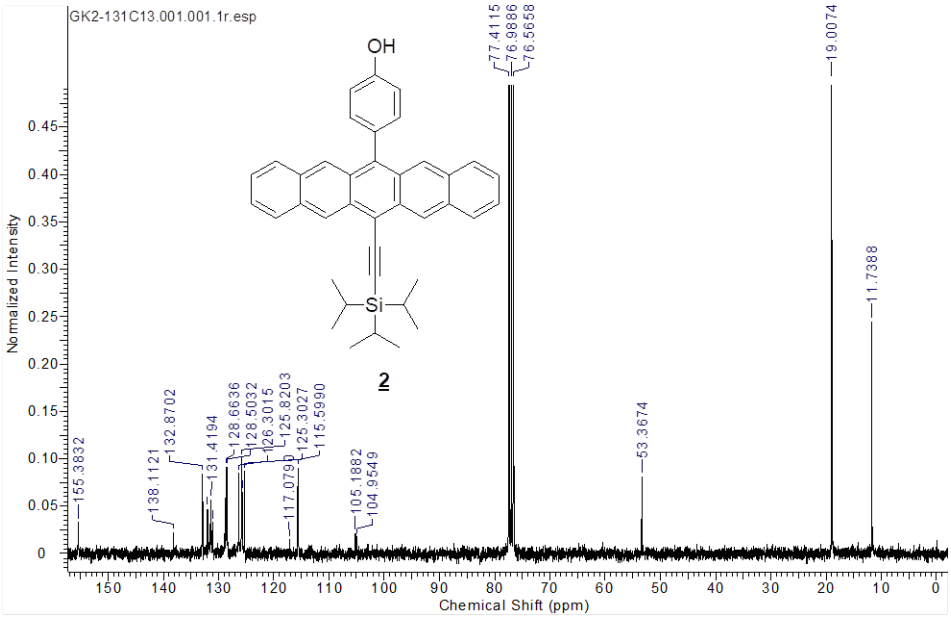

Figure S2: ^{13}C NMR (75.5 MHz, $CDCl_3$) spectrum of **2**.

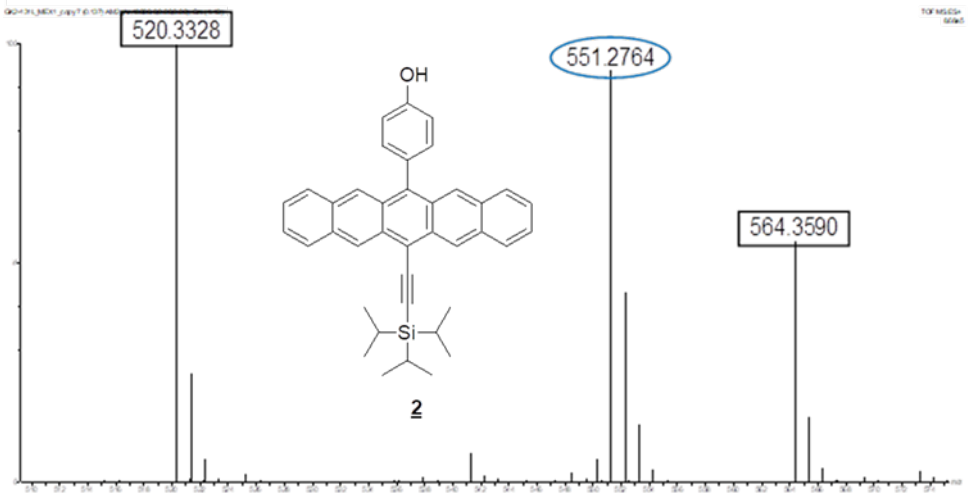

Figure S3: ESI-HRMS spectrum of **2** (peaks indicated with black box correspond to reference peaks for HRMS calibration).

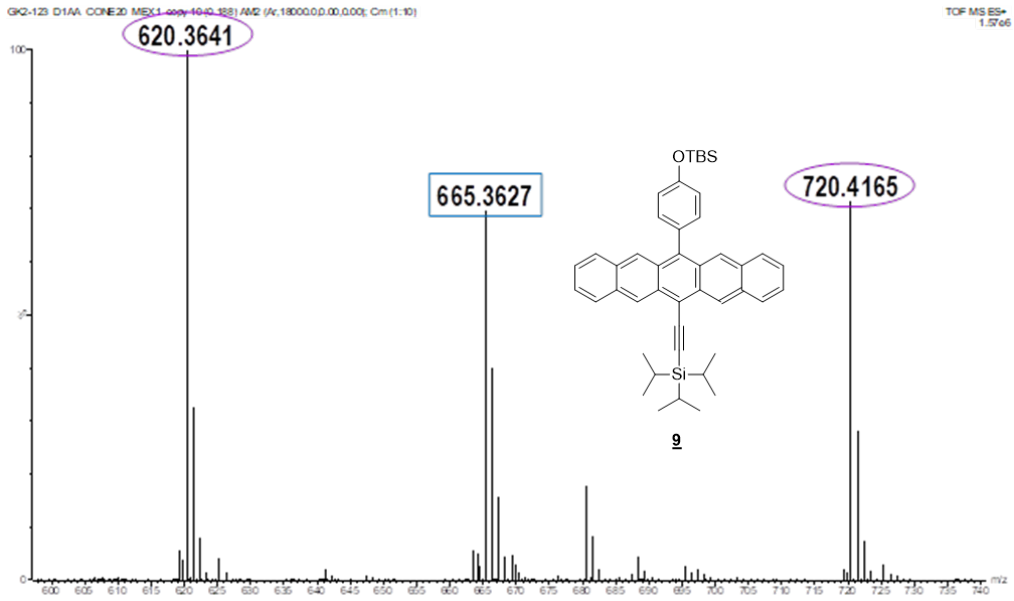

Figure S3-1: ESI-HRMS spectrum of **9** (peaks indicated with pink box correspond to reference peaks for HRMS calibration).

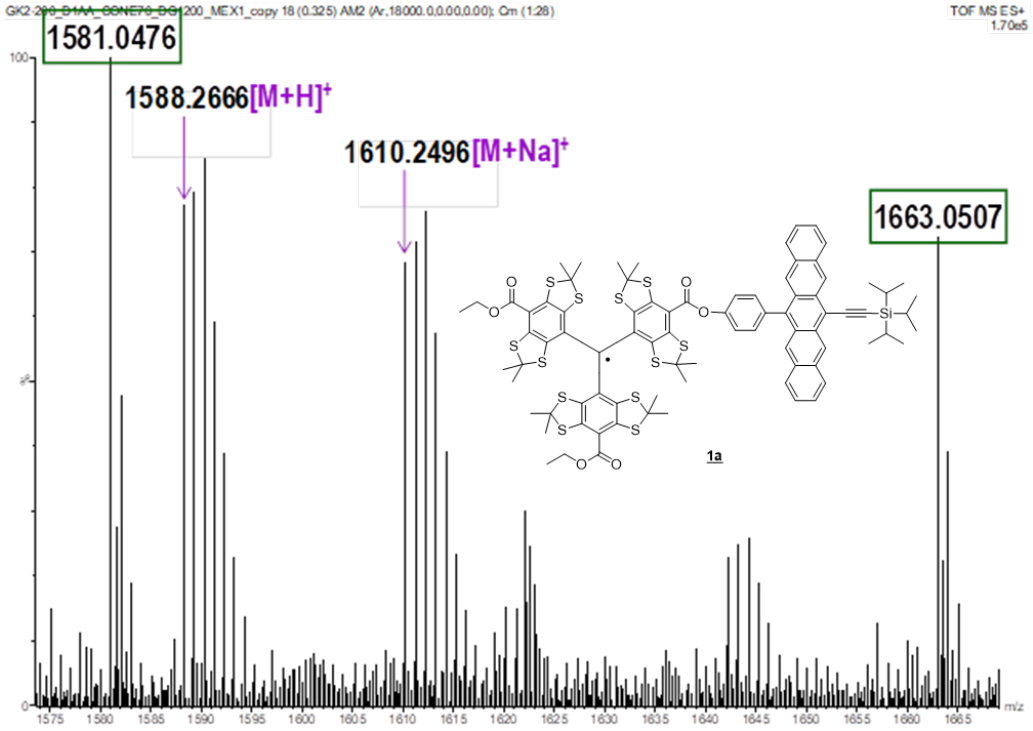

Figure S4: ESI-HRMS spectrum of **pTrityl <u>1a</u>** (peaks indicated with green box correspond to reference peaks for HRMS calibration).

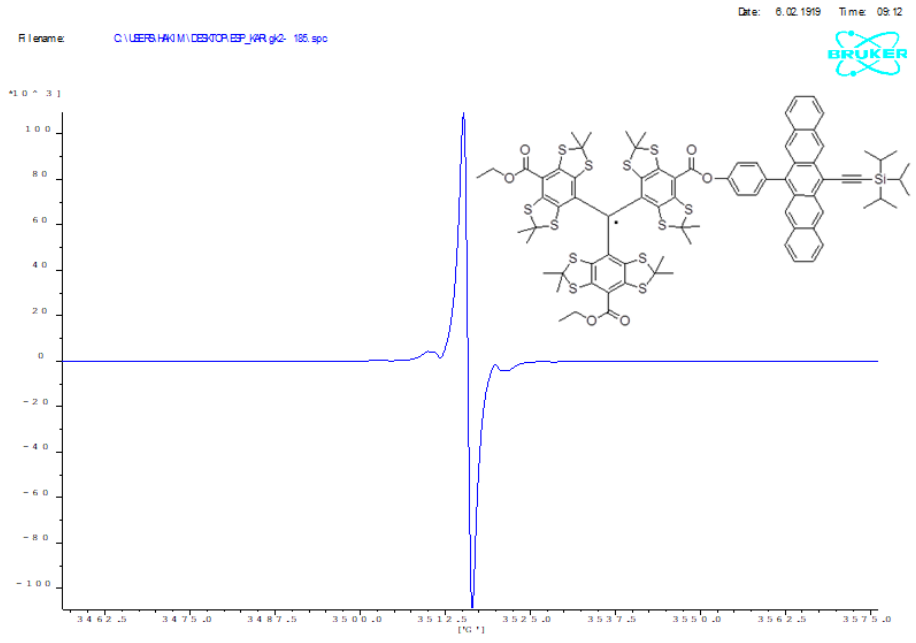

Figure S5: X-band EPR spectrum of **pTrityl <u>1a</u>** in dichloromethane.

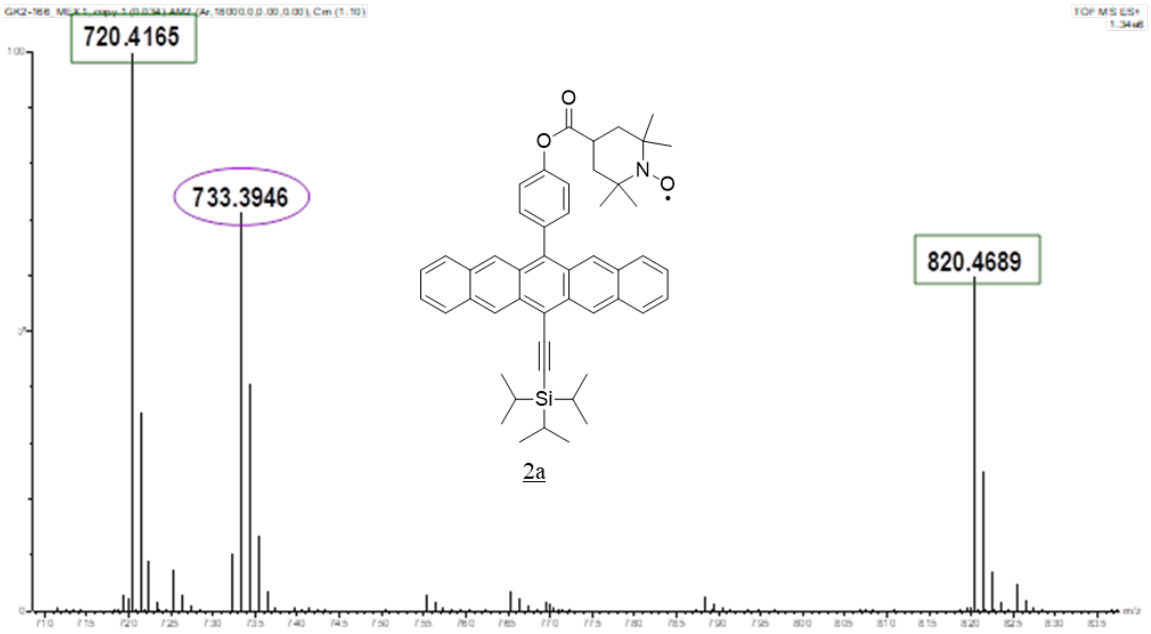

Figure S6: ESI-HRMS spectrum of **pTEMPO 2a** (peaks indicated with green box correspond to reference peaks for HRMS calibration).

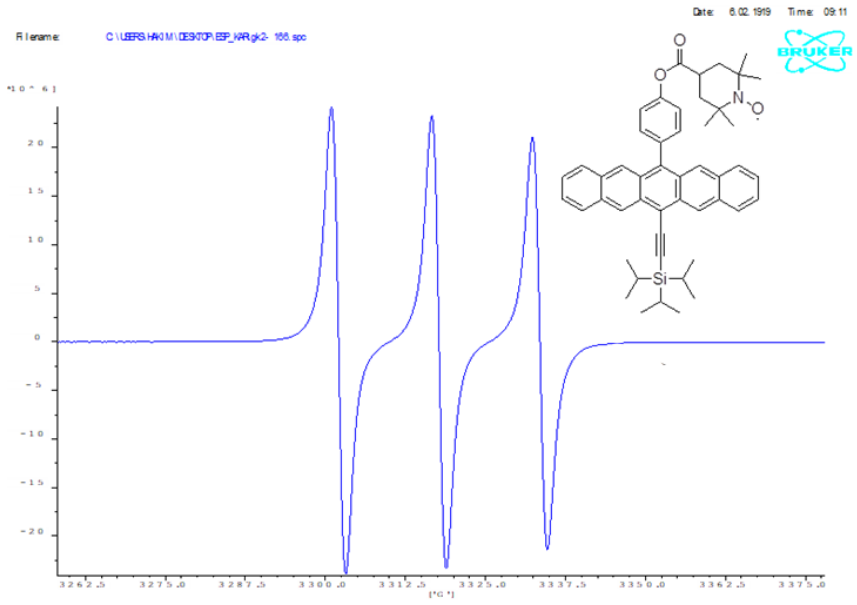

Figure S7: X-band EPR spectrum of **pTEMPO 2a** in dichloromethane**.**

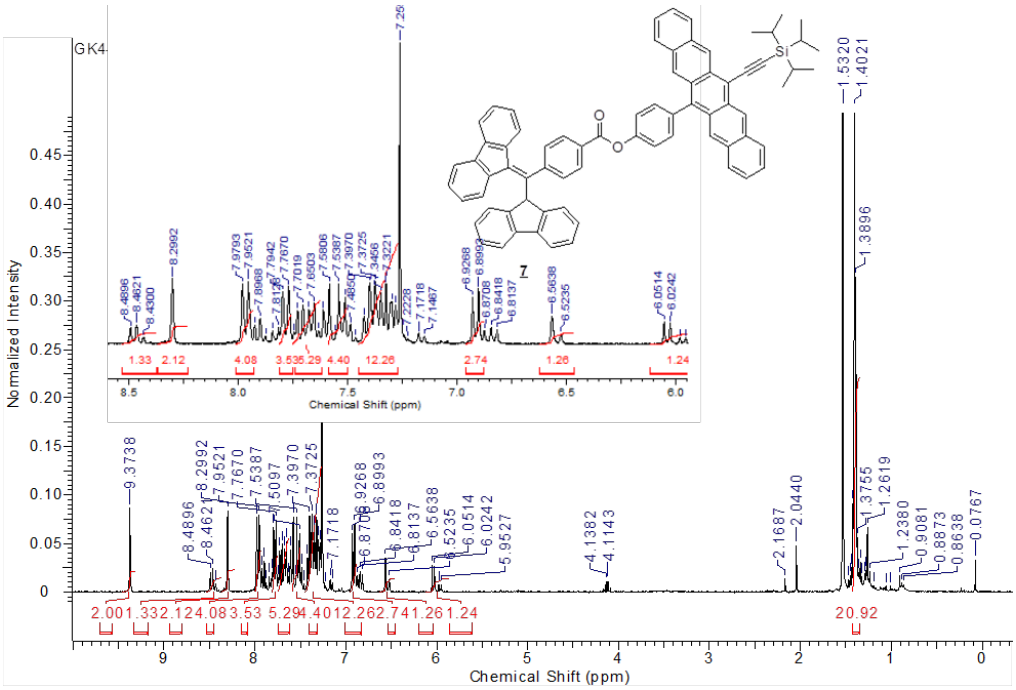

Figure S8: ^{1}H NMR (300 MHz, $CDCl_3$) spectrum of **7.**

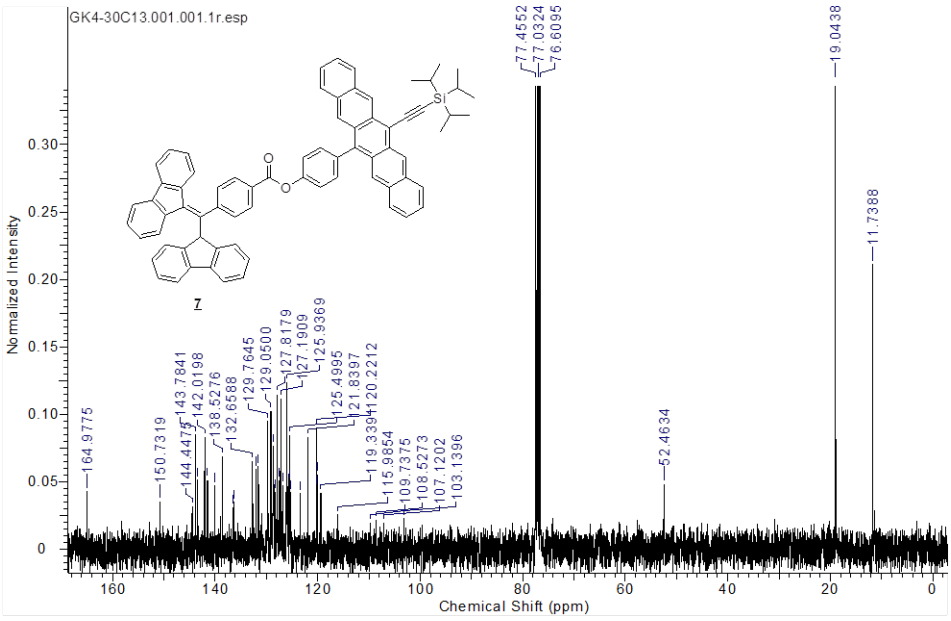

Figure S9: ^{13}C NMR (75.5 MHz, $CDCl_3$) spectrum of **7**.

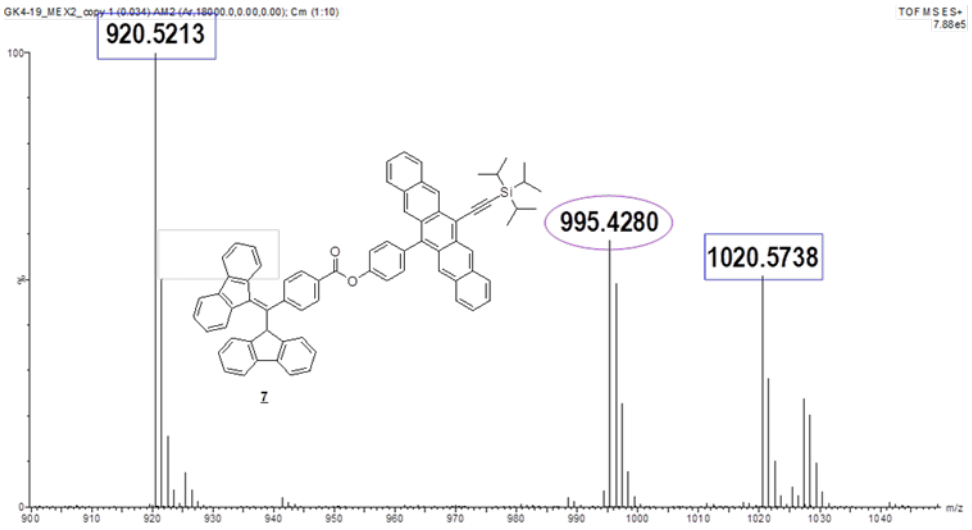

Figure S10: ESI-HRMS spectrum of **7** (peaks indicated with blue box correspond to reference peaks for HRMS calibration).

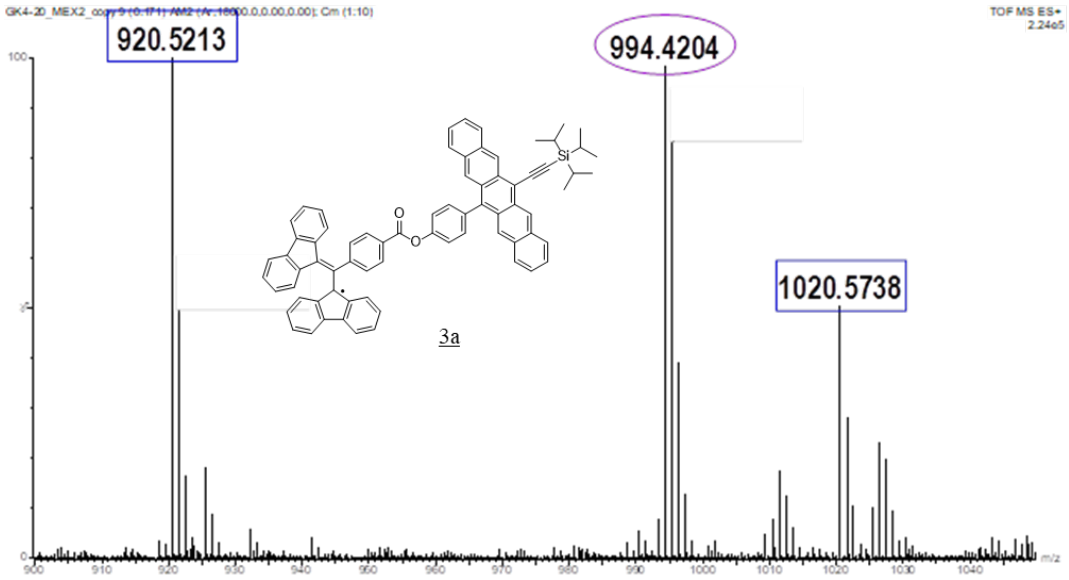

Figure S11: ESI-HRMS spectrum of **pBDPA 3a** (peaks indicated with green box correspond to reference peaks for HRMS calibration).

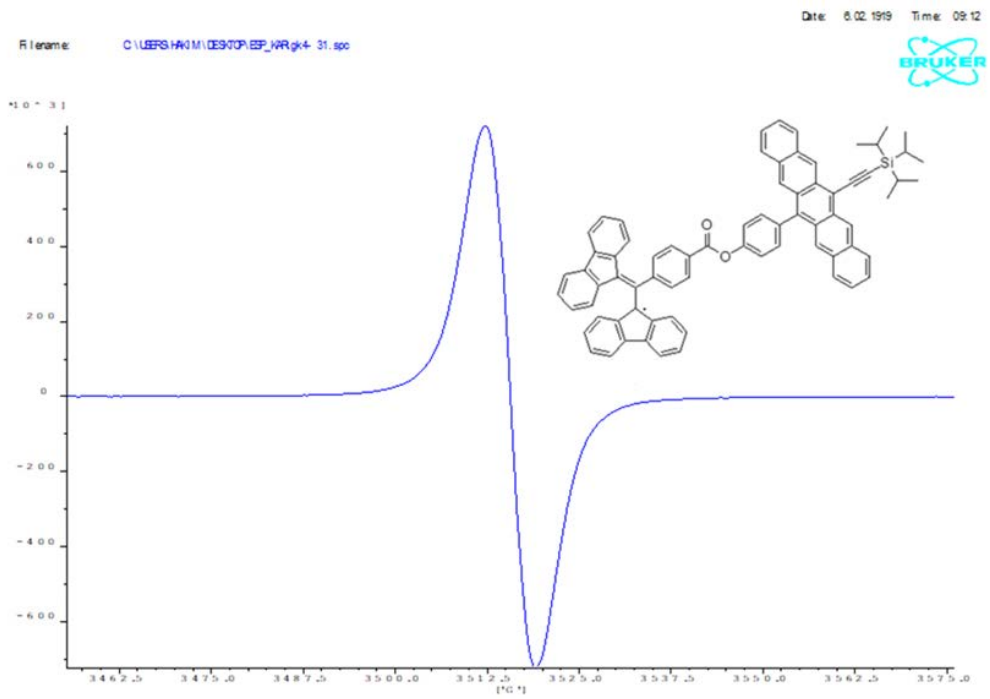

Figure S12: X-band EPR spectrum of **pBDPA <u>3a</u>** in dichloromethane.

2. Transient absorption spectroscopy

Ultrafast transient absorption (TA) spectra of pentacene derivatives were acquired using femtosecond pump-probe spectroscopy with a pump wavelength λ_{ex} = 600 nm.

The pump beam was obtained by pumping a two-stage non-colinear optical parametric amplifier (NOPA) with the output of a chirped pulse amplified Ti:sapphire laser (CPA-2001, Clark-MXR, λ = 778 nm, 120 fs pulse duration, 1 kHz repetition rate). Pump pulses were compressed to 39 fs FWHM duration by a pair of SF10 prisms. The dynamics of the photoinduced signals were obtained with a computer-controlled delay-line on the pump path. The pump beam was chopped at half of the laser frequency (500 Hz) and set at a magic angle (54.7°) with respect to the probe.

The probe beam was generated by directing a part of the 778 nm fundamental output of the laser into a CaF_2 crystal, yielding a white light continuum over a 400-780 nm wavelength domain. The probe beam was split before the sample into a beam overlapping with the pump beam on the sample (signal beam) and a reference beam. The probe fluence at the sample was much lower than that of the pump (11.5 $\mu J/cm^2$). Similarly, the diameter of the probe beam was smaller to ensure homogeneous excitation of the probed area.

Both signal and reference beams were guided to respective spectrographs (Princeton Instruments, Spectra Pro 2150i) and detected pulse-to-pulse with 512 x 58 pixels back-thinned CCD detectors (Hamamatsu S07030-0906)[4]. An average of 4,000 spectra per time delay. The time resolution of the experiment was 350 fs. Sample solutions were purged before the measurement with an argon-gas stream for 30 min to prevent degradation of the sample. The signal intensity coming from the photoinduced absorption was compared before and after each measurement.

2.1 Chirp correction and data treatment

The chirp mathematical correction was done with a MATLAB routine. The program extracts a Gaussian function corresponding to the instrument response function (IRF) for every wavelength. The wavefront of these Gaussian profiles is then fitted with a monoexponential function: $f(x) = y_0+A*\exp[-(x-x_0)/t]$ to extract the time zero for each wavelength. Then the corrected data were extracted from the initial file and treated separately using the Igor Pro software.

2.2 Global analysis

Global fits of the transient absorption data were carried out in this study to evaluate the singlet excited state dynamics. A comprehensive review of global analysis can be found in references[5-6].

In the present case, the decay process is fitted with a convolution of a biexponential decay and the IRF as displayed in eq. 1. We selected the latter equation since a two steps process is expected to explain the singlet excited state decay: a fast thermalization of the coherent excitation (solvation) followed by a slower relaxation of the excited state (mainly due to intersystem crossing).

$$I(t) = \left[A_1 e^{-t/\tau_1} + A_2 e^{-t/\tau_2}\right] \otimes IRF$$

Eq.1: Applied fitting function for the singlet excited state decay.

The following procedure was executed point per point:

1) Extraction of kinetic traces every 1 nm between 430 nm and 460 nm.
2) Fitting of the individual peak maximum trace to obtain good initial parameters for step 3.
3) Global fitting:
    a. Link the amplitude coefficients and the time constants for all the traces.
    b. Input initial parameters obtained in step 2.
    c. Perform fit with a given amount of iterations (here 100).
    d. Determine the fit efficiency by checking the residuals and by an individual fitting of the peak maximum.
4) Extraction of the amplitude coefficients and the time constants.

The IRF models the laser pump pulse (a Gaussian pulse with a FWHM of 350 ns).

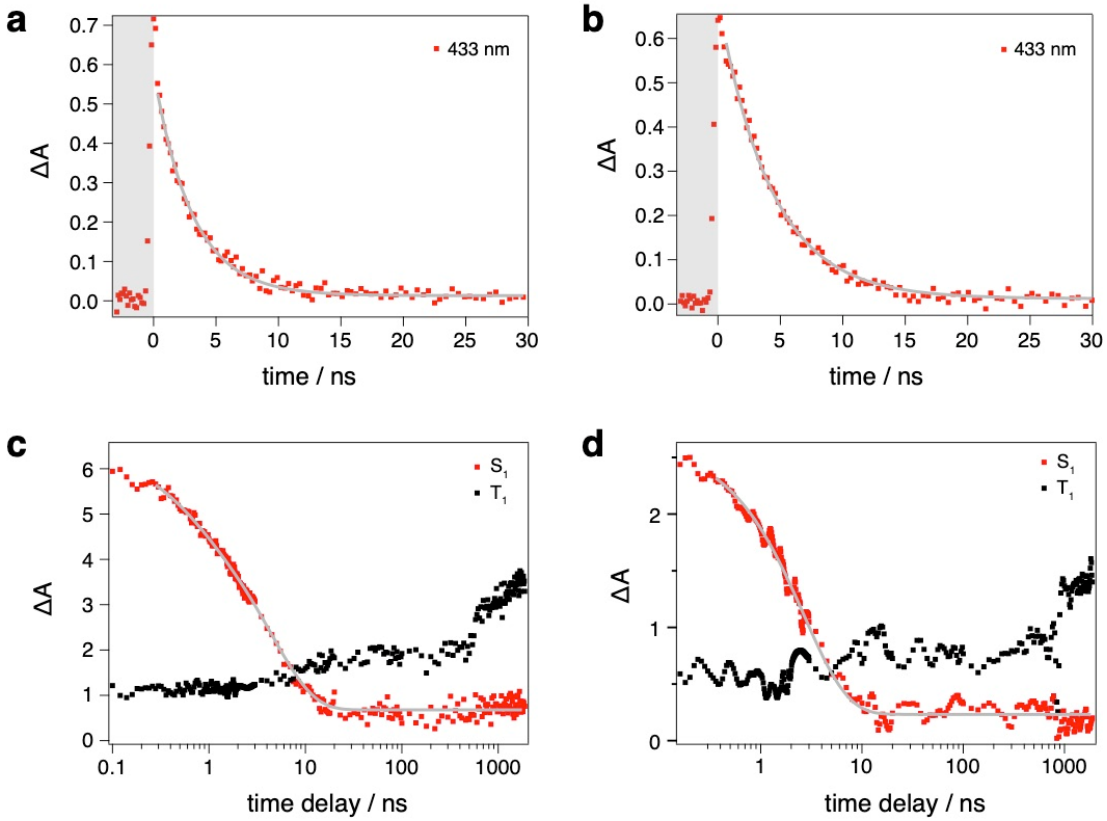

Figure S13: Evolution of the S_1 (λ=433 nm, red dots) and T_1 (λ=505 nm, black dots) states over time and the best-fit curve according to the procedure described above (grey line) of a) pBDPA, b) pTEMPO, c) pTrityl in butyronitrile and d) pTrityl in toluene.

3. EPR measurements

The solution-state EPR measurements shown in Figures S5, S7, S12 were taken in solutions of dichloromethane at room temperature. The solid-state EPR spectra were field-corrected using a BDPA field standard (g = 2.00242) and frequency-corrected to 9.75 GHz (see the main text and figure captions for conditions). Though we note that the spectral resolution at X-band is not sufficient to well-resolve the g-tensor and therefore does not afford a great deal of accuracy, which might explain why these values do not match well with literature values[15-17].

3.1 Pulsed EPR Measurements

Table S1. Fitted g-tensors from solid-state EPR measurements at 85 K in butyronitrile.

compound	[g_{xx} g_{yy} g_{zz}]
pTEMPO	[2.010, 2.005, 2.002]
pBDPA	[2.002, 2.004, 1.999]
pTrityl	[2.003, 2.003, 2.001]

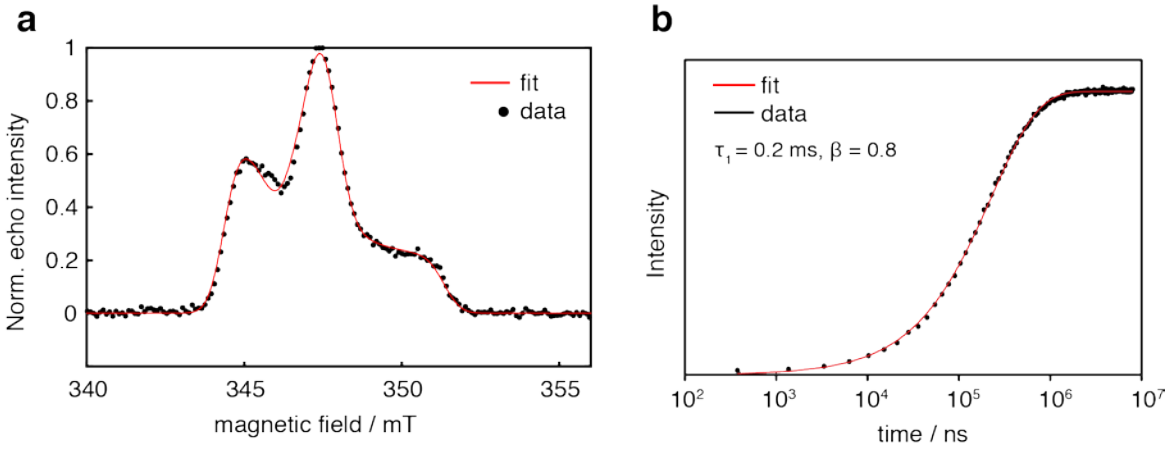

Figure S14: (a) X-Band field-swept echo-detected EPR measurement and fit of pTEMPO in butyronitrile at 85 K. The fit parameters are discussed in the text below. (b) T_1 measurement (saturation recovery) recorded at a field position corresponding to the intensity maximum fit with a biexponential.

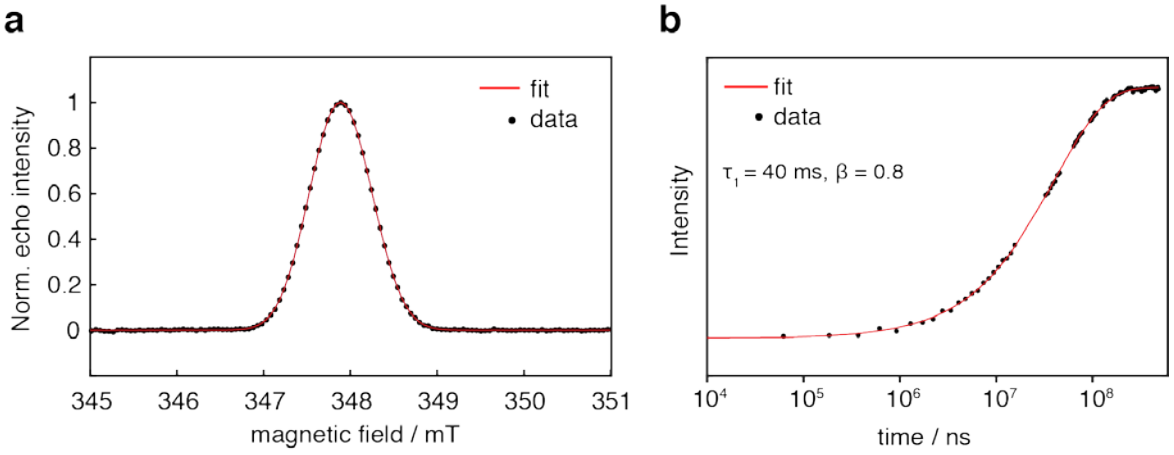

Figure S15: (a) X-Band field-swept echo-detected EPR measurement and fit of pBDPA in butyronitrile at 85 K. The fit parameters are discussed in the text below. (b) T_1 measurement at a field position corresponding to the intensity maximum fit with a stretched exponential.

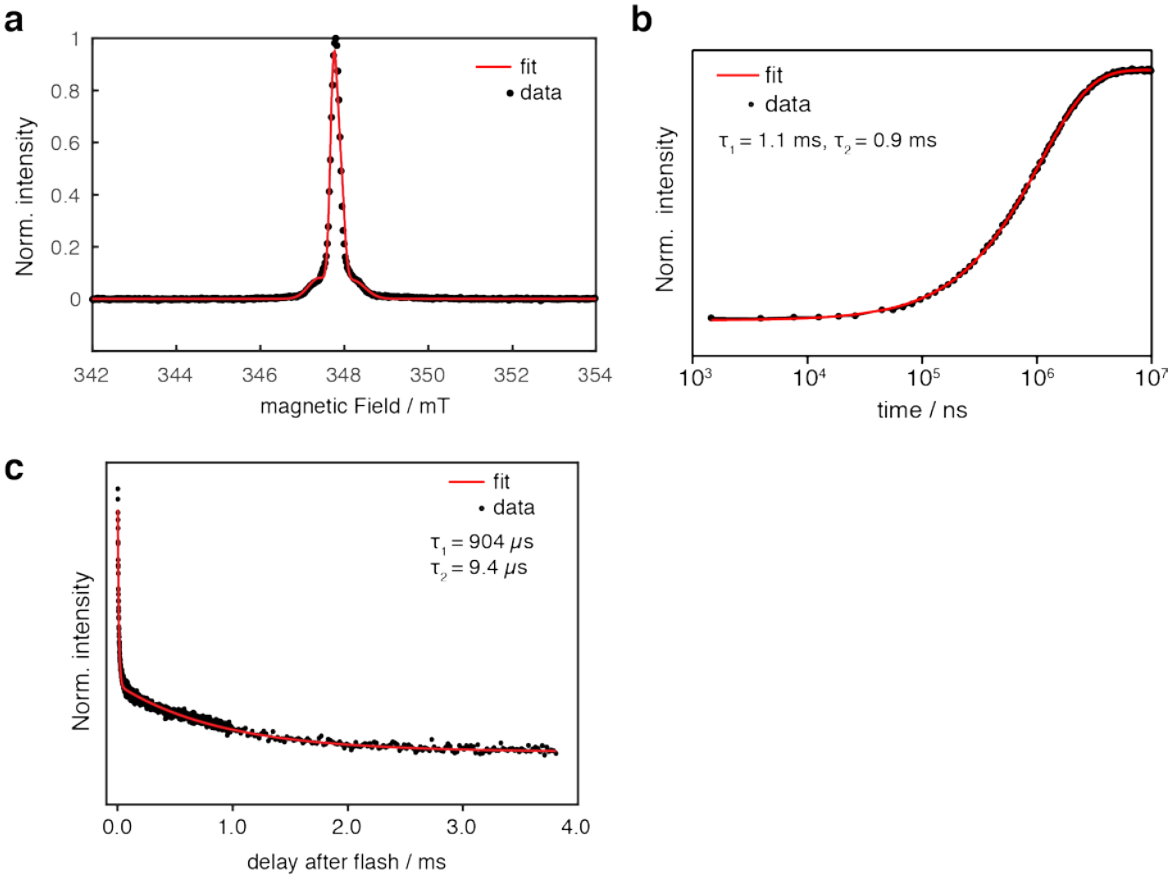

Figure S16: (a) X-Band free induction decay (FID)-detected EPR measurement and fit of pTrityl in butyronitrile at 85 K. The fit parameters are discussed in the text below. (b) T_1 measurement at a field position corresponding to the intensity maximum fit with a biexponential. (c) Decay of the spin polarization on trityl after laser excitation (delay after flash) at the X-band. 5 ns, 2 mJ pulse at 610 nm set to the EPR signal intensity maximum. Fit to biexponential decay model of f(x) = a*exp(–x/b) + c*exp(–x/d) to obtain a decay time constant of b = 900 µs with 95% confidence intervals (844, 924) µs and d = 9.4 (9.1, 9.6) µs, a = 0.77 (0.75, 0.78); c = 0.255 (0.253, 0.257), note that in this case the error distribution is not symmetric.

The T_1 measurements were fit using a biexponential or stretched exponential to account for a distribution of T_1 values across the sample, these values are reported in Figures S14, S15 and S16.

For the case of pTEMPO we fit using EasySpin's esfit function with pepper using principal **g**-tensor values of [2.0109, 2.0052, 2.0020] with ^{14}N hyperfine values of [23 15 96] MHz for the x, y and z principal axes, respectively, and a line broadening of 0.97 mT. For the case of pBDPA, g-factors of [2.0024, 2.0044, 1.9999] were used for the fit, with a line broadening of 0.68 mT. We did not explicitly include any contribution from hyperfine interactions in the simulations. The contribution of any unresolved ^{1}H couplings, leading to a homogeneous broadening of the lineshape[7], is accounted for in the overall linewidth. For the case of pTrityl, g-values of [2.0034, 2.0034, 2.0017] were used for the fit with ^{13}C hyperfine values of [19 28] MHz, [$A_{\parallel}$ $A_{\perp}$]. Figure S16a shows satellite transitions from the main peak that can be attributed to hyperfine coupling between the trityl and neighboring ^{13}C spins. Previous work suggests that this could also be due to dipolar coupling between the electron spins and ^{1}H spins on the trityl that lead to proton spin flip effects[8-10].

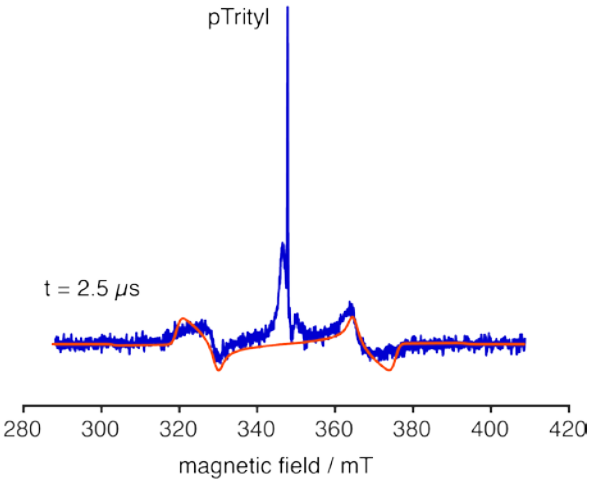

Figure S16-1: Triplet simulation superimposed on the TREPR spectrum of pTrityl in butyronitrile recorded at 2.5 µs after laser excitation.

The spectrum shown in figure S16-1 was simulated with the following parameters:

```
sys.S = 1;
sys.g = [2.0015, 2.0009, 2.0005]
sys.D = [1270 -100];
sys.lw = [1 0.2];
sys.HStrain = [50 50 50];
p= [0 0.7 0.3];
```

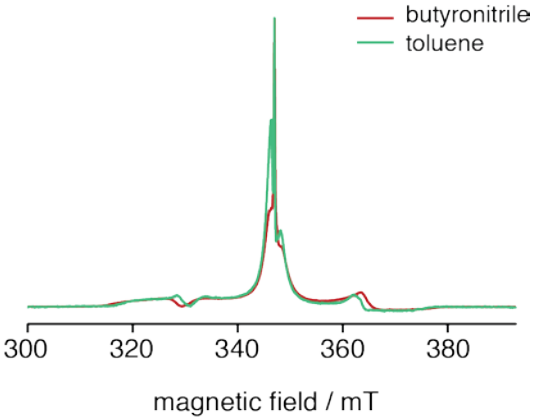

Figure S16-2: pTrityl in butyronitrile compared to pTrityl in toluene, both spectra show similar spectral features after laser excitation.

3.2 Field-swept echo-detected EPR of closed-shell pentacene derivative precursors

In the main text we show pulse EPR measurements on the open-shell pentacene derivative compounds **1a**, **2a** and **3a.** We also investigated the EPR properties of the closed-shell pentacene derivative pOTBS **9,** the precursor molecule for **1a, 2a** and **3a,** in an effort to obtain information about triplet yields. We then compared pOTBS to a model system, pTES **10,** shown in Figure S17.

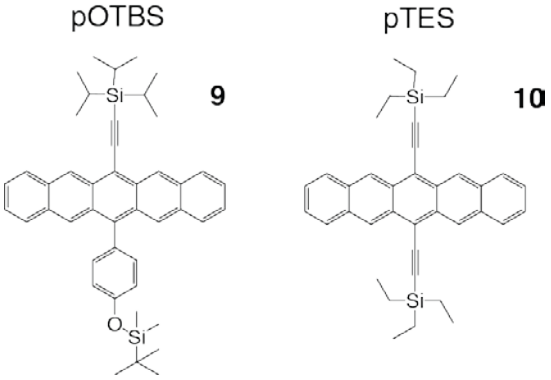

Figure S17. Precursor molecules, pOTBS **9** and pTES **10**.

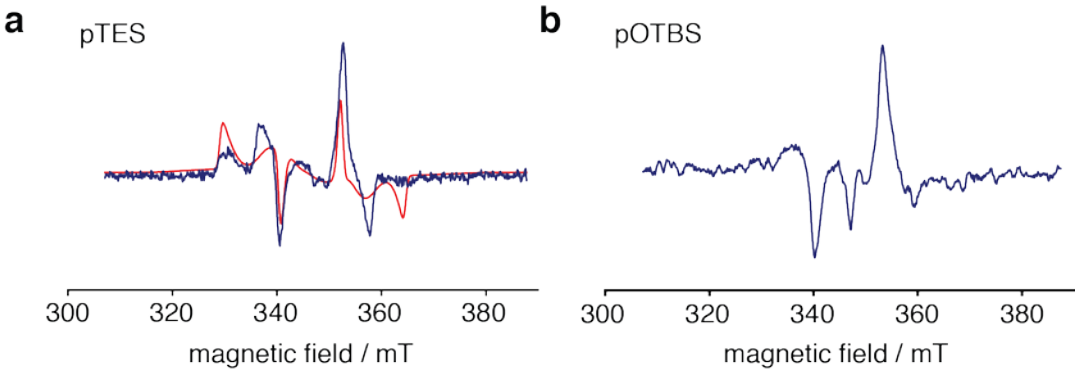

Figure S18: Field-swept echo-detected EPR spectra recorded in frozen butyronitrile at 85 K of (a) 0.5 mM pentacene-TES after photoexcitation at 630 nm together with an overlayed quintet fit and (b) of 0.5 mM pentacene-OTBS excited at 630 nm.

We observe a unique absorption and emission profile for our test compound pTES and precursor compound pOTBS. The pOTBS data is superimposed with a moving average of the same dataset for visual purposes due to the low SNR of the original dataset. We note that both the non-tethered pentacene-OTBS and pentacene-TES exhibit EPR spectra that might be indicative of quintet formation. We were unable to fit the TREPR spectra of the pentacene derivatives using a triplet model. We hypothesize that this may be due to aggregation effects (i.e. formation of triplet-triplet complexes) as stacking of two molecules may lead to delocalization of electrons across two molecules and therefore a set of different zero field splittings[11]. The quintet fit is overlaid in red in Figure S18a. We used the following fit parameters:

```
Sys.S = 2;
Sys.g = [2.0087 2.0045 2.0030];
Sys.D = [290 -13]; %MHz
Exp.Temperature = [1 1 0 0 1];
Sys.HStrain = [3 88 107];
```

Sys.lw = 0.8; %mT

Although the fit is not perfect, it suggests aggregate formation and close proximity between two triplets. The absorption and emission profiles seen in Figure S18 are quite similar to the transient ESR spectra of quintet states formed via strongly interacting triplet pairs in dilute pentacene films and TIPS-tetracene thin film systems[12-14]. In addition, the similar absorption and emission profiles of the quintet states in pTES and pOTBS indicate little change in the selectivity of intersystem crossing into spin sublevels for pTES and pOTBS.

3.4 Estimation of local electron spin polarization enhancement

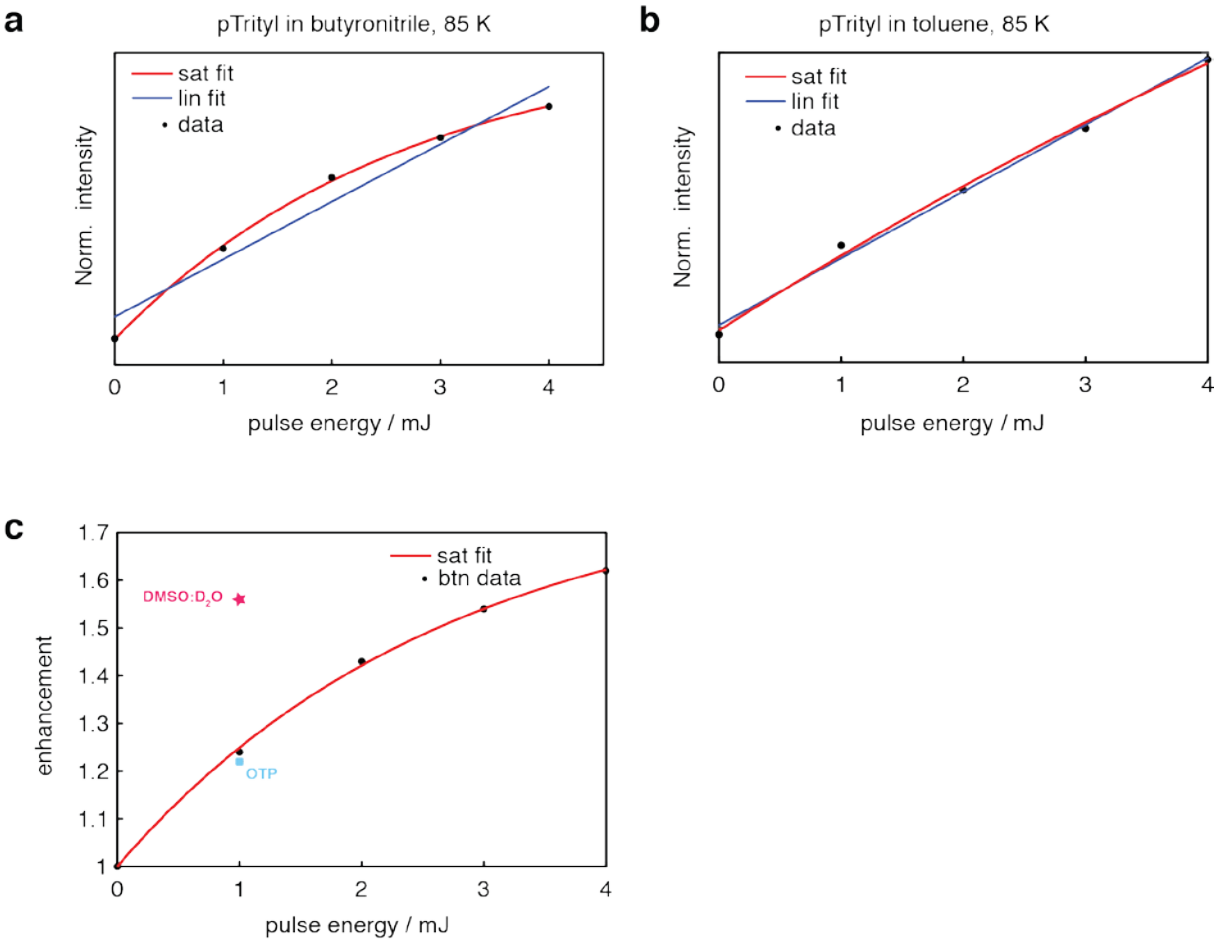

Figure S18-1: Integrated normalized FID intensity of pTrityl as a function of excitation energy in (a) btn and (b) tol. (c) Integrated enhancement (photoexcitation on/photoexcitation off) as a function of excitation energy in btn. The signals were integrated over a field range covering the intensity maximum (345 to 349 mT).

Figure S18-1 shows normalized integrated signal intensities of pTrityl at four different laser pulse excitation energies in butyronitrile and toluene. For the case of butyronitrile, an exponential fit gives an $R^2 = 0.99$ while the linear fit gives $R^2 = 0.95$, which suggests that 4 mJ is in the limit of saturation. This calibration was done to investigate whether samples were saturated in order to obtain an upper limit on the local enhancement. From the exponential fit, at 4 mJ we obtain 89% of the maximum possible signal enhancement. For the case of toluene, an exponential fit gives the same R^2 value as the linear fit indicating that saturation is not obtained until much higher powers for this sample.

The calculation is a simplification and serves simply to give an order of magnitude estimate since we do not take into account the change in the beam diameter through the sample. We assume a laser spot

size of 2 mm, 0.1 mM pTrityl in butyronitrile with active detection volume of 70 µL. Only about 67% of the molecules in the volume contribute to the absorption at this wavelength if one considers the approximate molar absorptivity for a similar system[13], the EPR tube path length and sample concentration. We calculate the illuminated volume and divide by the total volume. We calculated a maximum EPR signal enhancement of 1.6 by comparing the EPR signal intensity of light on divided by light off (cf. main text), and we assume that the sample is homogeneously distributed and that the enhancement in the total EPR signal comes only from the illuminated volume. From this we can write out a simple equation where I is the illuminated volume, A is the active volume, E is the observed EPR signal enhancement and e_{local} is the local enhancement.

$$E = \frac{A\left(1 - \frac{I}{A}\right) + A\left(\frac{I}{A}\right) e_{local} * 0.67}{A}$$

Which simplifies to:

$$E = \left(1 - \frac{I}{A}\right) + \left(\frac{I}{A}\right) e_{local}$$

From this calculation we obtain a lower limit on the local enhancement factor e_{local} of ~ 10.

4. UV-vis absorption spectroscopy

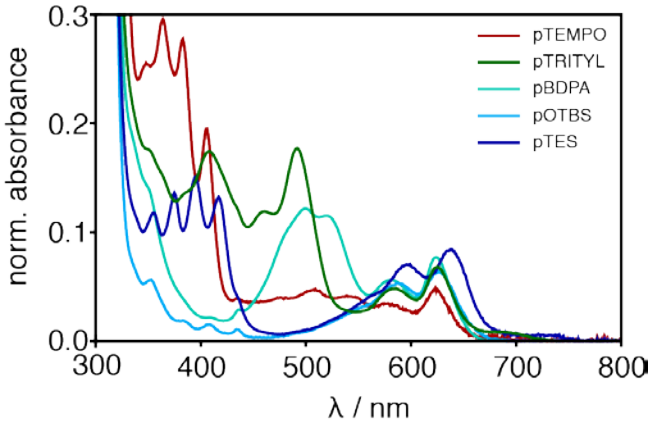

Figure S19. UV-vis spectra of pTEMPO, pBDPA, pTrityl, pTES and pOTBS in toluene. The pentacene derivatives containing radicals are blue-shifted with respect to pentacene TES in toluene.

5. References

1. Lehnherr, D.; Gao, J.; Hegmann, F. A.; Tykwinski, R. R., Synthesis and Electronic Properties of Conjugated Pentacene Dimers. *Org. Lett.* **2008**, *10*, 4779-4782.
2. Dane, E. L.; Maly, T.; Debelouchina, G. T.; Griffin, R. G.; Swager, T. M., Synthesis of a BDPA-TEMPO Biradical. *Org. Lett.* **2009**, *11*, 1871-1874.
3. Reginsson, G. W.; Kunjir, N. C.; Sigurdsson, S. T.; Schiemann, O., Trityl Radicals: Spin Labels for Nanometer-Distance Measurements. *Chem. Eur J.* **2012**, *18*, 13580-13584.
4. Bouduban, M. E. F.; Burgos-Caminal, A.; Ossola, R.; Teuscher, J.; Moser, J. E., Energy and Charge Transfer Cascade in Methylammonium Lead Bromide Perovskite Nanoparticle Aggregates. *Chem. Sci.* **2017**, *8*, 4371-4380.

5. van Stokkum, I. H. M.; Larsen, D. S.; van Grondelle, R., Global and Target Analysis of Time-Resolved Spectra. *Biochim. Biophys. Acta.* **2004**, 1657, 82–104.
6. Berera, R.; van Grondelle, R.; Kennis, J. T. M., Ultrafast Transient Absorption Spectroscopy: Principles and Application to Photosynthetic Systems. *Photosynth. Res.* **2009**, *101*, 105-118.
7. Can, T. V.; Caporini, M. A.; Mentink-Vigier, F.; Corzilius, B.; Walish, J. J.; Rosay, M.; Maas, W. E.; Baldus, M.; Vega, S.; Swager, T. M.; Griffin, R. G., Overhauser Effects in Insulating Solids. *J. Chem. Phys.* **2014**, *141*, 0642021-0642028.
8. Lumata, L.; Kovacs, Z.; Sherry, A. D.; Malloy, C.; Hill, S.; van Tol, J.; Yu, L.; Song, L. K.; Merritt, M. E., Electron Spin Resonance Studies of Trityl Ox063 at a Concentration Optimal for DNP. *Phys. Chem. Chem. Phys.* **2013**, *15*, 9800-9807.
9. Trammell, G. T.; Zeldes, H.; Livingston, R., Effect of Environmental Nuclei in Electron Spin Resonance Spectroscopy. *Phys. Rev.* **1958**, *110*, 630-634.
10. Bowman, M. K.; Mailer, C.; Halpern, H. J., The Solution Conformation of Triarylmethyl Radicals. *J. Magn. Reson.* **2005**, *172*, 254-267.
11. Thurnauer, M. C.; Katz, J. J.; Norris, J. R., Triplet-State in Bacterial Photosynthesis - Possible Mechanisms of Primary Photo-Act. *PNAS*, **1975**, *72*, 3270-3274.
12. Weiss, L. R.; Bayliss, S. L.; Kraffert, F.; Thorley, K. J.; Anthony, J. E.; Bittl, R.; Friend, R. H.; Rao, A.; Greenham, N. C.; Behrends, J., Strongly Exchange-Coupled Triplet Pairs in an Organic Semiconductor. *Nat. Phys.* **2017**, *13*, 176-181.
13. Chernick, E. T.; Casillas, R.; Zirzlmeier, J.; Gardner, D. M.; Gruber, M.; Kropp, H.; Meyer, K.; Wasielewski, M. R.; Guldi, D. M.; Tykwinski, R. R., Pentacene Appended to a Tempo Stable Free Radical: The Effect of Magnetic Exchange Coupling on Photoexcited Pentacene. *J. Am. Chem. Soc.* **2015**, *137*, 857-863.
14. Lubert-Perquel, D.; Salvadori, E.; Dyson, M.; Stavrinou, P. N.; Montis, R.; Nagashima, H.; Kobori, Y.; Heutz, S.; Kay, C. W. M., Identifying Triplet Pathways in Dilute Pentacene Films. *Nat. Commun.* **2018**, *9*, 1-10.
15. Trukhan, S. N.; Yudanov, V. F.; Tormyshev, V. M.; Rogozhnikova, O. Y.; Trukhin, D. V.; Bowman, M. K.; Krzyaniak, M. D.; Chen, H.; Martyanov, O. N., Hyperfine Interactions of Narrow-Line Trityl Radical with Solvent Molecules. *J. Magn. Reson.* **2013**, *233*, 29-36.
16. Dupeyre, R. M.; Lemaire, H.; Rassat, A., Nitroxides. XIV. A Stable Biradical in Nitroxide Series. *J. Am. Chem. Soc.* **1965**, *87*, 3771-3772.
17. Dane, E. L.; Swager, T. M., Synthesis of a Water-Soluble 1,3-Bis(Diphenylene)2-Phenylallyl Radical. *J. Org. Chem.* **2010**, *75*, 3533-3536.